NASA/CR-1998-208963
ICASE Report No. 98-55

A Gas-kinetic Scheme for Reactive Flows

Yongsheng Lian
The Hong Kong University of Science and Technology, Hong Kong

Kun Xu
ICASE, Hampton, Virginia
and
The Hong Kong University of Science and Technology, Hong Kong

Institute for Computer Applications in Science and Engineering
NASA Langley Research Center
Hampton, VA

Operated by Universities Space Research Association

National Aeronautics and
Space Administration

Langley Research Center
Hampton, Virginia 23681-2199

Prepared for Langley Research Center
under Contract NAS1-97046

December 1998

A GAS-KINETIC SCHEME FOR REACTIVE FLOWS *

YONGSHENG LIAN † AND KUN XU ‡

Abstract. In this paper, the gas-kinetic BGK scheme for the compressible flow equations is extended to chemical reactive flow. The mass fraction of the unburnt gas is implemented into the gas kinetic equation by assigning a new internal degree of freedom to the particle distribution function. The new variable can be also used to describe fluid trajectory for the nonreactive flows. Due to the kinetic governing equation, the current scheme basically solves the Navier-Stokes chemical reactive flow equations. Numerical tests validate the accuracy and robustness of the current kinetic method.

Key words. Boltzmann equation, kinetic scheme, reactive flow

Subject classification. Applied Numerical Methods

1. Introduction. There are mainly two numerical approaches to the solution of the compressible Euler equations, namely, the Godunov and the Boltzmann schemes. Broadly speaking, the Godunov scheme is based on the Riemann solution and characteristics play an important role in the description of the gas evolution. However, the Boltzmann scheme uses the microscopic particle distribution function as the basis in the construction of the flux function and the Euler solution is considered as a limiting case when the particle collision time goes to zero. The Godunov and the Boltzmann schemes are based on two different physical interpretations of flow motion. Due to the possible implementation of nonequilibrium gas property in the kinetic scheme, both the robustness and accuracy of the scheme can be maintained [10].

In this paper, we extend the gas-kinetic BGK scheme for the nonreactive compressible Euler equations to the reactive flows. In order to implement the mass fraction into the kinetic formulation, one new internal degree of freedom z is implemented in the gas distribution function. For nonreactive flows, this function can be also used for the tracking of fluid trajectory. In the reactive flow calculations, we are only accounting for two species, which are the unburnt and burnt gases. The unburnt gas is converted to burnt gas via a simple irreversible reaction process. As a special application, the new scheme is used in the study of detonation waves in both 1-D and 2-D cases.

The inviscid reacting compressible Euler equations in 1-D case are

$$\begin{cases} \rho_t + (\rho U)_x = 0, \\ (\rho U)_t + (\rho U^2 + p)_x = 0, \\ (\rho Z)_t + (\rho Z U)_x = -\rho K(T) Z, \\ (\rho \epsilon)_t + (\rho \epsilon U + pU)_x = q_0 \rho K(T) Z, \end{cases} \tag{1.1}$$

where ρ is the density, U the velocity, p the pressure, Z the mass fraction of unburnt gas, and q_0 is the amount of heat released per unit mass by reaction. The total energy density is $\rho\epsilon = \frac{1}{2}\rho U^2 + \rho e$, where ρe is the internal energy. We assume that both unburnt and burnt gases have the same γ. The equation of state

*This research was supported by the National Aeronautics and Space Administration under NASA Contract No. NAS1-97046 while the author was in residence at the Institute for Computer Applications in Science and Engineering (ICASE), NASA Langley Research Center, Hampton, VA 23681-2199. Additional support was provided by Hong Kong Research Grant Council through RGC97/98.HKUST6166/97P

†Mathematics Department, The Hong Kong University of Science and Technology, Hong Kong (email:malian@uxmail.ust.hk).

‡Mathematics Department, The Hong Kong University of Science and Technology, Hong Kong (email:makxu@uxmail.ust.hk); and ICASE, Mail Stop 403, NASA Langley Research Center, Hampton, VA 23681-2199 (email: kxu@icase.edu).

can be expressed as $p = \rho TR/m$, where R is the gas constant and m is the molecular mass. $K(T)$ is the chemical reactive rate, which is a function of temperature. The specific form of $K(T)$ will be given in the numerical section.

Many researchers have been working on the numerical solution of equations (1.1). A partial list of references includes Colella et.al. [2], Lindstrom [6], Engquist and Sjogreen [3], and Jeltsch and Klingenstein [4]. Mostly, a splitting scheme is used to solve the above equations and the flow variables inside each cell are updated through

$$\frac{dW_j}{dt} = \frac{1}{\Delta x}(F_{j-1/2}(t) - F_{j+1/2}(t)) + S(W_j),$$

where $W_j = (\rho, \rho U, \rho Z, \rho\epsilon)_j^T$ is the cell-averaged conservative variables, $S = (0, 0, -\rho K(T)Z, q_0\rho K(T)Z)_j^T$ is the source term, and the flux function $F_{j+1/2}$ is obtained by solving Eq.(1.1) without considering the source term. In this paper, a gas-kinetic model and the corresponding kinetic scheme for the evaluation of the flux function $F_{j+1/2}$ of the homogeneous Euler equations will be presented, and the source term $S(W_j)$ in the above equation is treated implicitly for the update of flow variables W_j inside each cell.

2. A Gas-Kinetic Model. A gas-kinetic BGK model for Eq.(1.1) without the source terms can be constructed as the following equation,

$$f_t + uf_x = \frac{g - f}{\tau}, \tag{2.1}$$

where f is the gas-distribution function, u the particle velocity, and $Q(f, f) = (g - f)/\tau$ the particle collision term [1]. The equilibrium state g has the form,

$$g = \rho\left(\frac{\lambda}{\pi}\right)^{\frac{K+2}{2}} e^{-\lambda((u-U)^2+(z-Z)^2+\xi^2)},$$

where K is the number of dimensions of the internal variable ξ and is related to γ,

$$K = (3 - \gamma)/(\gamma - 1),$$

and $\xi^2 = \xi_1^2 + \xi_2^2 + ... + \xi_K^2$. The term λ is a function of the gas temperature T with the relation $\lambda = m/2KT$ and k is the Boltzmann constant.

The connection between the distribution function f and the macroscopic flow variables is

$$(\rho, \rho U, \rho Z, \rho\epsilon)^T = \int \psi_\alpha f dudzd\xi,$$

where $d\xi = d\xi_1 d\xi_2 ... d\xi_K$ and

$$\psi_\alpha = (1, u, z, \frac{1}{2}(u^2 + \xi^2))^T$$

are the moments for density ρ, momentum ρU, mass fraction ρZ, and total energy $\rho\epsilon$. The fluxes for the corresponding macroscopic variables are

$$(F_\rho, F_{\rho U}, F_{\rho Z}, F_{\rho\epsilon})^T = \int u\psi_\alpha f dudzd\xi.$$

For the homogeneous flow equations (1.1) without the source terms, the compatibility condition of the collision term in the Boltzmann equation is

$$\int Q(f, f)\psi_\alpha dudzd\xi = \begin{pmatrix} 0 \\ 0 \\ 0 \\ 0 \end{pmatrix}. \tag{2.2}$$

For the equilibrium flow with $f = g$, the homogeneous Euler equations with the inclusion of mass fraction can be recovered by taking the moments of ψ_α to Eq.(2.1),

$$\int \begin{pmatrix} 1 \\ u \\ z \\ \frac{1}{2}(u^2+\xi^2) \end{pmatrix} (g_t + ug_x) du dz d\xi = 0,$$

and the resulting equations become

$$\begin{pmatrix} \rho \\ \rho U \\ \rho Z \\ \frac{1}{2}\rho(U^2 + \frac{K+1}{2\lambda}) \end{pmatrix}_t + \begin{pmatrix} \rho U \\ \rho U^2 + \frac{\rho}{2\lambda} \\ \rho ZU \\ \frac{1}{2}\rho(U^3 + \frac{(K+3)U}{2\lambda}) \end{pmatrix}_x = 0.$$

So, the corresponding pressure is $p = \rho/2\lambda$ and the internal energy density ρe goes to

$$\rho e = \frac{(K+1)\rho}{4\lambda}.$$

To the first order of τ, the Chapman-Enskog expansion gives

$$f = g - \tau(g_t + ug_x),$$

and the BGK model automatically reduces to the Navier-Stokes equations,

$$\begin{pmatrix} \rho \\ \rho U \\ \rho Z \\ \frac{1}{2}\rho(U^2 + \frac{K+1}{2\lambda}) \end{pmatrix}_t + \begin{pmatrix} \rho U \\ \rho U^2 + \frac{\rho}{2\lambda} \\ \rho UZ \\ \frac{1}{2}\rho(U^3 + \frac{(K+3)U}{2\lambda}) \end{pmatrix}_x = \tau \begin{pmatrix} 0 \\ \frac{2K}{K+1}\frac{\rho}{2\lambda}U_x \\ \frac{\rho}{2\lambda}Z_x \\ \frac{K+3}{4}\frac{\rho}{2\lambda}(\frac{1}{\lambda})_x + \frac{2K}{K+1}\frac{\rho}{2\lambda}UU_x \end{pmatrix}_x, \tag{2.3}$$

where the dynamic viscous coefficient is $\eta = \tau p$. In the 2-D cases, similar viscous governing equations can be derived from the BGK model [10]. As a result, for the chemical reactive flows, the real governing equations solved by the kinetic BGK scheme are the reactive Navier-Stokes equations instead of inviscid equations (1.1). This is basically one of the direct reason for the robustness of kinetic BGK scheme.

Remark: in the above equations, the function Z has no dynamical effect on the gas evolution, it only provides additional information about the flow property, which can be the mass fraction for the reactive flow, level set function for the interface tracking, color function for the fluid trajectory capturing, and the pollution concentration for certain gas species.

3. Gas-Kinetic Flow Solver . In order to evaluate the numerical fluxes across a cell interface $x_{j+1/2}$, we need to get the gas distribution function there. The general solution of f at the cell interface $x_{j+1/2}$ and time t is

$$f(x_{j+1/2}, t, u, z, \xi) = \frac{1}{\tau}\int_0^t g(x', t', u, z, \xi) e^{-(t-t')/\tau} dt' + e^{-t/\tau} f_0(x_{j+1/2} - ut), \tag{3.1}$$

where $x' = x_{j+1/2} - u(t-t')$ is the trajectory of the particle motion and f_0 is the initial gas distribution function f at the beginning of each time step ($t = 0$). Two unknowns, g and f_0 in Eq.(3.1), have to be addressed in the above equation in order to obtain the explicit form of f.

Generally, the distributions of f_0 and g around the cell interface $x_{j+1/2}$ and time $t = 0$ are obtained using the Taylor expansion of the Maxwellian distribution function, for example

$$f_0 = \begin{cases} g^l\left(1 + a^l(x - x_{j+1/2})\right), & x \le x_{j+1/2} \\ g^r\left(1 + a^r(x - x_{j+1/2})\right), & x \ge x_{j+1/2} \end{cases} \tag{3.2}$$

and

$$g = g_0 \left(1 + (1 - \mathrm{H}[x - x_{j+1/2}])\bar{a}^l(x - x_{j+1/2}) + \mathrm{H}[x - x_{j+1/2}]\bar{a}^r(x - x_{j+1/2}) + \bar{A}t\right), \tag{3.3}$$

where g^l, g^r and g_0 are local Maxwellians located at the left, right and middle of a cell interface. The parameters $a^l, a^r, \bar{a}^l, \bar{a}^r$ have the following form

$$a = a_1 + a_2 u + a_3 z + a_4(u^2 + \xi^2),$$

and all parameters (a_1, a_2, a_3, a_4) can be found from the slopes of the corresponding macroscopic variables. $\mathrm{H}[x]$ is the Heaviside function defined as

$$H[x] = \begin{cases} 0, & x < 0 \\ 1, & x \geq 0 \end{cases}.$$

The reason and detailed formulation in the determination of f_0 is presented in [12, 10]. The only difference here is that we need to use the macroscopic distribution ρZ in the determination of the $a_3 z$ term.

After f_0 is obtained, the equilibrium state g_0 at a cell interface

$$g_0 = \rho_0 (\frac{\lambda_0}{\pi})^{\frac{K+2}{2}} e^{-\lambda_0((u-U_0)^2 + (z-Z_0)^2 + \xi^2)},$$

is determined as follows. Taking the limit of $t \to 0$ in Eq.(3.1) and substituting its solution into Eq.(2.2), the compatibility constraint at $(x = x_{j+1/2}, t = 0)$ gives

$$W_0 = \int g_0 \psi_\alpha du dz d\xi = \int_{u>0} \int g^l \psi_\alpha du dz d\xi + \int_{u<0} \int g^r \psi_\alpha du dz d\xi.$$

Similarly the corresponding slopes of g in Eq.(3.3) can be obtained from the macroscopic slopes between the cell averaged flow quantities W_j and W_{j+1} and the above value W_0 at the cell interface [12].

After substituting Eq.(3.2) and Eq.(3.3) into Eq.(3.1), the final gas distribution function at a cell interface is

$$\begin{aligned} f(x_{j+1/2}, t, u, z, \xi) = {} & (1 - e^{-t/\tau})g_0 + \left(\tau(-1 + e^{-t/\tau}) + te^{-t/\tau}\right)\left(\bar{a}^l \mathrm{H}[u] + \bar{a}^r(1 - \mathrm{H}[u])\right) u g_0 \\ & + \tau(t/\tau - 1 + e^{-t/\tau})\bar{A} g_0 \\ & + e^{-t/\tau}\left((1 - uta^l)\mathrm{H}[u]g^l + (1 - uta^r)(1 - \mathrm{H}[u])g^r\right). \end{aligned} \tag{3.4}$$

The only unknown in the above equation is $\bar{A}$ term, which is determined by implementing the compatibility condition over the whole time step Δt at the location $x_{j+1/2}$,

$$\int_0^{\Delta t} \int (g(x_{j+1/2}, t, u, z, \xi) - f(x_{j+1/2}, t, u, z, \xi)) dt du dz d\xi = 0.$$

There is no iteration involved in the determination of $\bar{A}$ from the above equation [12]. After f is obtained, the time-dependent numerical fluxes in the x-direction across the cell interface can be computed as

$$\begin{pmatrix} \mathcal{F}_\rho \\ \mathcal{F}_{\rho U} \\ \mathcal{F}_{\rho Z} \\ \mathcal{F}_{\rho \epsilon} \end{pmatrix}_{j+1/2} = \int u \begin{pmatrix} 1 \\ u \\ z \\ \frac{1}{2}(u^2 + \xi^2) \end{pmatrix} f(x_{j+1/2}, t, u, z, \xi) du dz d\xi. \tag{3.5}$$

By integrating the above equation over the whole time step Δt, we get the total $W = (\rho, \rho U, \rho Z, \rho \epsilon)$ transport.

4. Numerical Examples. In the numerical examples reported in this section, the van Leer limiter is used for the reconstruction of conservative variables W at the beginning of each time step. Unless specifically stated, the gas constant γ is equal to 1.4. The first three test cases are about the nonreactive flow and the mass fraction is used as an interface tracer for the fluid evolution; the following two test cases are about 1-D and 2-D detonation wave calculations.

Case(1): Diffusion of mass fraction function

As analyzed in section 2, the real governing equation obtained from the kinetic BGK model for the function ρZ is the advection diffusion equation,

$$(\rho Z)_t + (\rho U Z)_x = \tau(\frac{\rho}{2\lambda} Z_x)_x.$$

In order to test the above governing equation, we set two uniform initial flow conditions with

$$(\rho = 1, p = 1, U = 0), \quad \text{and} \quad (\rho = 1, p = 1, U = 0.5). \tag{4.1}$$

The computational domain consists of 200 grid points with cell size $\Delta x = 1.0$. The function Z is initially assigned with the value

$$Z = \begin{cases} -1, & x < 100, \\ 1. & x \geq 100. \end{cases}$$

Two fixed collision times $\tau = 0.03$ and $\tau = 0.015$ are used in the computations, which correspond to viscosity coefficients $\nu = 0.03$ and $\nu = 0.015$ respectively. At the output time $t = 100$, the numerical and exact solutions for both cases are shown in Fig.(5.1). The results confirm that the BGK scheme does solve the advection diffusion equation for the mass fraction function Z.

Case(2) Fluid trajectory in the shock tube case [9]

The forward-facing case is carried out on a uniform mesh of 120×40 cells and $\Delta x = \Delta y = 1/40$. We choose the color function Z at the inlet $x = 0$ with the following boundary conditions

$$Z = \begin{cases} 1.0 & \text{for } 0 \leq y < \frac{3}{40}, \\ -1.0 & \text{for } \frac{3}{40} \leq y < \frac{21}{40}, \\ 1.0 & \text{for } \frac{21}{40} \leq y < \frac{33}{40}, \\ -1.0 & \text{for } \frac{33}{40} \leq y < 1. \end{cases}$$

The computed density and pressure distributions are presented in Fig.(5.2). In the same figure, the contours of function Z are added, from which the interfaces between different "colored" fluid and the fluid trajectories can be clearly observed. For example, the fluid particles change direction after passing through the oblique shock.

Case(3) Rayleigh-Taylor instability [7, 5]

This computation is performed on a rectangular domain of $x \in [0, 1]$ and $y \in [0, 2]$ with reflecting boundary conditions on the lower and upper sides of the domain and periodic ones in the horizontal direction. The gravity is directed downward with dimensionless gravitational constant $G = 0.5$.

The densities next to the initial fluid interface at $y = 1$ are $\rho_1 = 0.5$ and $\rho_2 = 1.0$ with the ratio $\rho_2/\rho_1 = 2 : 1$, and the functions Z are 1.0 below the interface and -1.0 above that. The value of the pressure at the fluid interface ($y = 1$) is $1/1.4$, and isothermal conditions are used to determine flow distributions in both the upper and lower parts. The initial density perturbation at the interface is added with the form $\delta\rho = 0.05(1 - \cos(2\pi x))$. Since the heavy fluid is located on top of the light fluid, it stays in an unstable

situation when the system is subjected to gravity. The computed contours of function Z with the values $Z = [-0.5, 0.0, 0.5]$ at output time $t = 10.0$ on three different mesh sizes ($\Delta x = \Delta y = 1/64, 1/128, 1/192$) are shown in Fig.(5.3). Since the collision time $\tau = 4 \times 10^{-4}$ is fixed in all these three cases, the physical viscosity coefficient $\tau p/\rho$ keeps the same value. Therefore, even with the mesh refinement the simulation results are basically identical. If the Riemann solution of the inviscid Euler equations is used in the flux evaluation $F_{j+1/2}$, the numerical results usually do not converge with the mesh-refinement [7]. The nonconvergence of the numerical results is more serious for the detonative reactive flows using the exact Godunov method [8, 6].

Case(4) 1-D denotation wave

In this case, we are going to study the formation of the ZND wave for the following reaction kinetics,

$$K(T) = \begin{cases} K_0, & T \geq T_0, \\ 0, & T < T_0, \end{cases} \tag{4.2}$$

where T_0 is the ignition temperature and K_0 the reaction rate. This specific case is taken from [4]. The initial data are piece-wise constant, which defines the Chapman-Jouget detonation wave:

$$(\rho_l = 1.9690 \times 10^{-3} \frac{g}{cm^3},\ U_l = 4.8057 \times 10^4 \frac{cm}{sec},\ p_l = 7.9434 \times 10^6 \frac{g}{cmsec^2},\ Z = 0),$$
$$(\rho_r = 1.2010 \times 10^{-3} \frac{g}{cm^3},\ U_l = 0.0,\ p_l = 0.8321 \times 10^6 \frac{g}{cmsec^2},\ Z = 1.0).$$

In the calculation, the gas constant R is equal to $8.3143 \times 10^7 cm^2 g/sec^2 K mol$, the molecular weight $m = 36 g/mol$, the ignition temperature $T_0 = 500^o K$, the reaction rate $K_0 = 0.582458 \times 10^{10}/s$, and the heat release $q_0 = 6.9283 \times 10^9 cm^2/sec^2$. The spatial step size Δx used in each case is varied according to $\Delta x = \alpha R_0$, where $R_0 = 5.347 \times 10^{-6} cm$ and the parameter α takes the values $0.01, 0.1, 1$ in the three cases. The results at subsequent times with different α are shown in Fig.(5.4)-(5.6). From these figures, we find that a detonation wave is a strong shock wave propagating into a reactant, followed by a thin zone of reaction which supports the shock.

Case(5) 2-D denotation wave [6]

As illustrated in [6], with the mesh refinement the reactive Euler solvers can generate unphysical solutions in the complicated oscillating detonation waves. The spurious solution appears even using the exact Godunov method [8].

The initial condition for the 2D denotation simulation is an exact traveling solution of the ZND wave. The reaction rate $K(T)$ has the following Arrhenius formulation,

$$K(T) = K_0 T^\alpha e^{-E/T}. \tag{4.3}$$

The parameters used are $q_0 = 50, E = 50, \gamma = 1.2$ and $\alpha = 0$. The reaction rate K_0 is set to be 10^4. The initial data is a one-dimensional ZND profile in the x-direction. The ZND wave connects the left state $\rho_l = 1.731379$, $U_l = 3.015113$ $V_l = 0$, $\rho_l \epsilon_l = 130.4736$, $Z_l = 0$ by a Chapman-Jouget detonation with the right state $\rho_r = 1, U_r = 0, V_R = 0, \rho_r \epsilon_r = 15, Z_r = 1$. The computational domain is 0.6×1.0, and the cell size used is $\Delta x = \Delta y = 1/400$. A periodic perturbation is imposed in the y-direction of the initial ZND profile, where the initial data $W(x, y, 0)$ is set to $W_{ZND}(x + \Delta x \mathrm{NINT}(\frac{0.05}{\Delta x} \cos(4\pi y)))$, where $\mathrm{NINT}(z)$ is the nearest integer close to z. The simulation results around the ZND wave front for the subsequent times from $5/64, 6/64, ..., 16/65$ are shown in the Fig.(5.7). From this figure, we can clearly see the oscillating profile of the ZND wave front and the "explosion within explosion " phenomena due to the collision of triple points.

For the Godunov scheme, due to the inadequate dissipation in the gas evolution stage, the shock instability and carbuncle phenomena are intrinsically rooted [11], and the robustness of the Godunov scheme can

hardly be achieved for the complicated flow system in the high resolution calculations, such as the chemical reactive and MHD equations. A detail analysis of the dissipative mechanism in the Godunov method is presented in [11]. However, for the gas-kinetic BGK scheme, we are basically solving the viscous governing equations even for the inviscid target equations. So, the robustness is well maintained. This kind of approach is physically founded, because we are obtaining the numerical solutions on the discretized space and time, where the spatial and temporal resolution is limited by the cell size and time step. The subcell smearing is equivalent to the intrinsic dissipation. In order to remove the unphysical solutions in Riemann solver based methods, the reactive Navier-Stokes equations are solved directly in [6]. However, the evaluation of the viscous terms requires substantial computation resources. In this aspect, the gas-kinetic scheme of the current paper is efficient since the viscous and heat conduction terms have been included in the gas distribution function (3.5) already.

5. Conclusion. In this paper, we have extended the BGK scheme to the chemical reactive flow with the inclusion of one more internal degree of freedom in the gas distribution function to account for the mass fraction. This mass function can be also used to track the fluid interfaces for the nonreactive flows. The numerical results confirm the robustness, accuracy and efficiency of the BGK method.

REFERENCES

[1] P.L. Bhatnagar, E.P. Gross, and M. Krook, *A Model for Collision Processes in Gases I: Small Amplitude Processes in Charged and Neutral One-Component Systems*, Phys. Rev., **94** (1954), pp. 511-525.

[2] P. Colella, A. Majda, and V. Roytburd, *Theoretical and Numerical Structure for Reacting Shock Wave*, SIAM J. Sci. Stat. Comput., **7** (1986), pp. 1059-1080.

[3] B. Engquist and B. Sjogreen, *Robust Difference Approximations of Stiff Inviscid Detonation Waves*, Research Report (1991), Computational and Applied Mathematics, UCLA.

[4] R. Jeltsch and P. Klingenstein, *Error Estimators for the Position of Discontinuities in Hyperbolic Conservation Laws with Source Terms Which are Solved Using Operator Splitting*, Research Report No. 97-16 (1997), ETH, Switzerland.

[5] A.D. Kotelnikov and D.C. Montgomery, *A Kinetic Method for Computing Inhomogeneous Fluid Behavior*, J. Comput. Phys., **134** (1997) , pp. 364-388.

[6] D. Lindstrom, *Numerical Computation of Viscous Detonation Waves in Two Space Dimensions*, Research Report (1996), Uppsala University, Department of Scientific Computing, Uppsala, Sweden.

[7] M. Mulder, S. Osher, and J.A. Sethian, *Computing Interface Motion in Compressible Gas Dynamics*, J. of Comput. Phys., **100** (1992), pp. 209-228.

[8] J. Quirk, *Godunov-type Schemes Applied to Detonation Flows*, ICASE Report 93-15 (1993).

[9] P. Woodward and P. Colella, *Numerical Simulations of Two-dimensional Fluid Flow with Strong Shocks*, J. Comput. Phys., **54** (1984), pp. 115.

[10] K. Xu, *Gas-Kinetic Schemes for Unsteady Compressible Flow Simulations*, 29th CFD Lecture Series, von Karman Institute for Fluid Dynamics (1998).

[11] K. Xu, *Gas-Evolution Dynamics in Godunov-type Schemes and Analysis of Numerical Shock Instability*, ICASE Report (1999).

[12] K. Xu, C. Kim, L. Martinelli, and A. Jameson, *BGK-based Schemes for the Simulation of Compressible Flow*, Int. J. of Comput. Fluid Dynamics, **7** (1996), pp. 213-235.

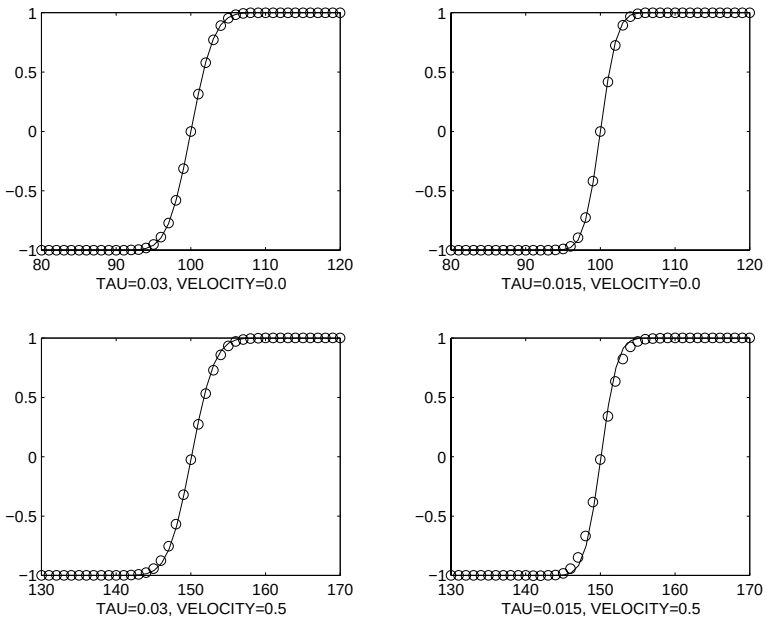

FIG. 5.1. *Propagation of function Z with velocity $U = 0$ (top) and $U = 0.5$ (bottom). The collision times used are $\tau = 0.03$ (left) and $\tau = 0.015$ (right) respectively. The solid lines are exact solutions and the circles are numerical solutions.*

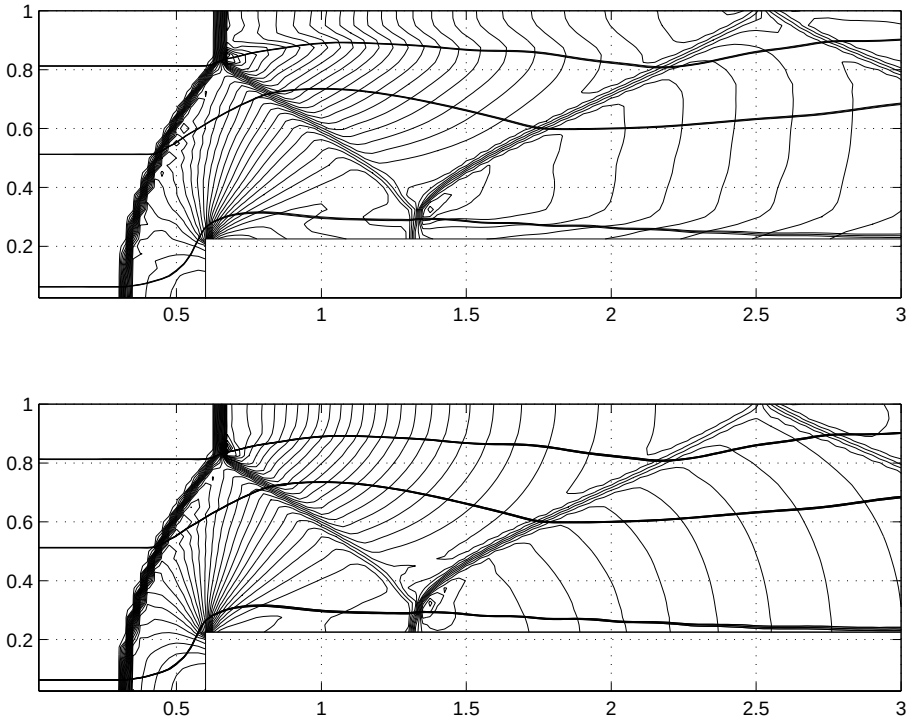

FIG. 5.2. *Density and pressure contours for the step case. The contours of function Z with $Z = [-1/32, 0, 1/32]$ are added in these plots to show the fluid trajectory. The mesh size used here is 120×40.*

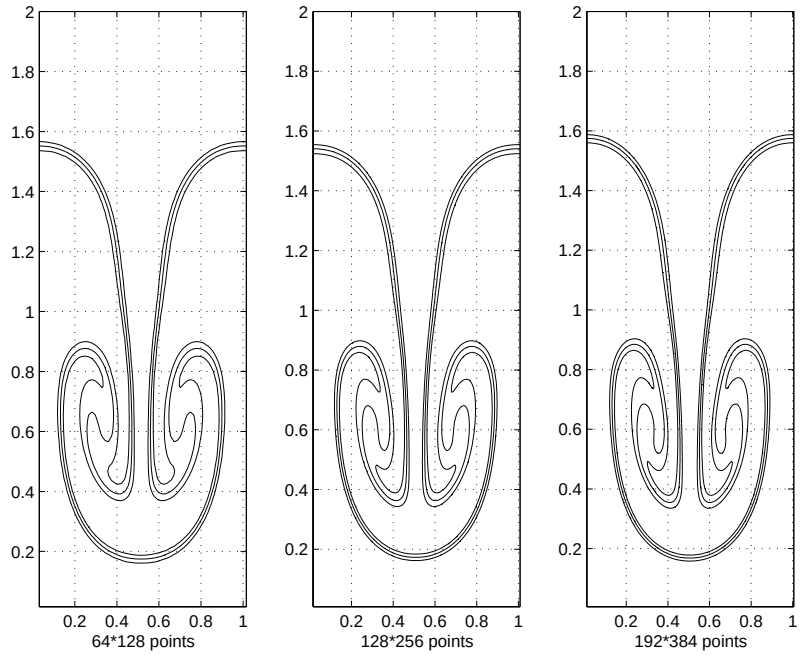

FIG. 5.3. *In the Rayleigh-Taylor instability case, the interface between the heavy and light fluid is captured with the help of function Z, and the contours have the values of $Z = [-0.5, 0.0, 0.5]$. From left to right, the mesh sizes used are $64 \times 128, 128 \times 256, 192 \times 384$ and the collision time in each case keeps the same value $\tau = 4 \times 10^{-4}$. Therefore, the physical viscous coefficient is the same, so are the simulation results.*

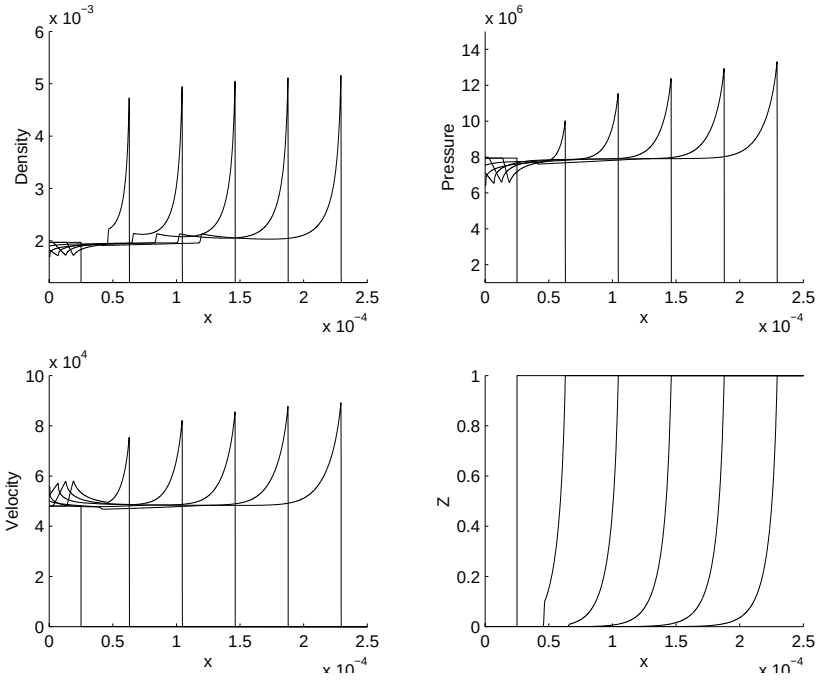

FIG. 5.4. *Density, pressure, velocity and mass fraction Z plots at time steps $0, 2000, ..., 10000$ with $\alpha = 0.01$.*

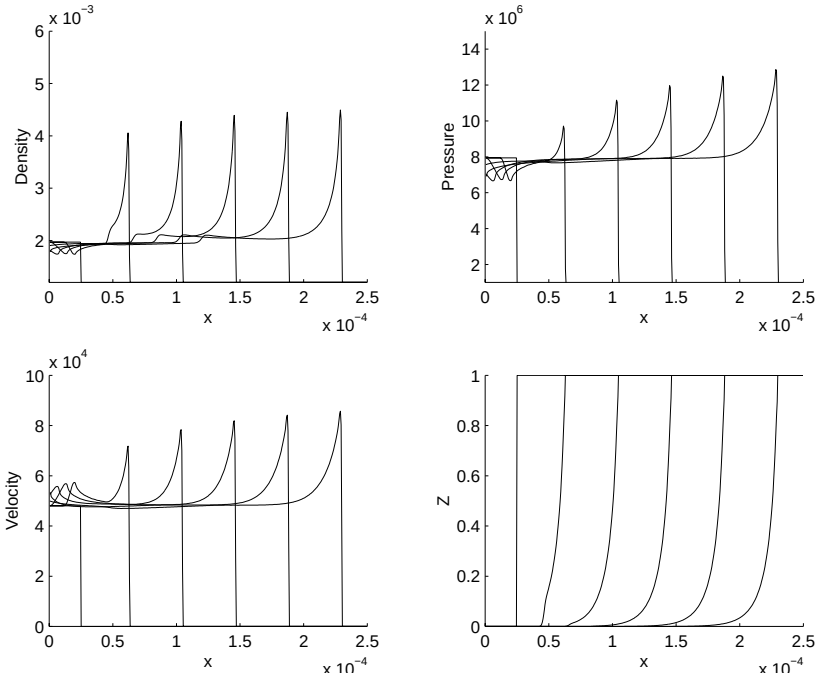

FIG. 5.5. *Density, pressure, velocity and mass fraction Z plots at time steps* $0, 2000, ..., 10000$ *with* $\alpha = 0.1$.

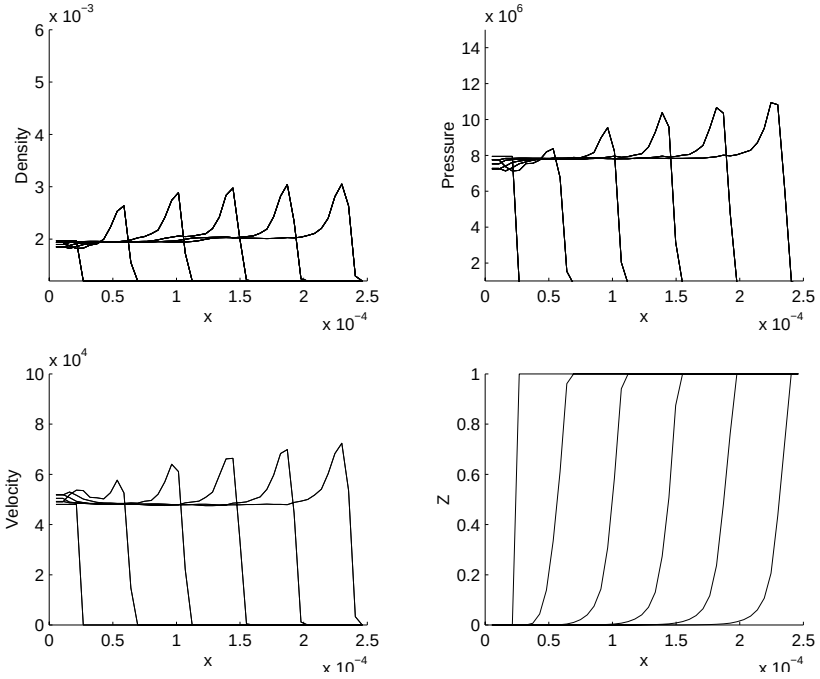

FIG. 5.6. *Density, pressure, velocity and mass fraction Z plots at time steps* $0, 2000, ..., 10000$ *with* $\alpha = 1$. *Due to the large cell size in this case, the peak values are reduced and the profiles get smeared in comparison with Fig.(5.4) and Fig.(5.5). If* α *is continuously increasing, spurious solutions of one cell per time step will appear [2].*

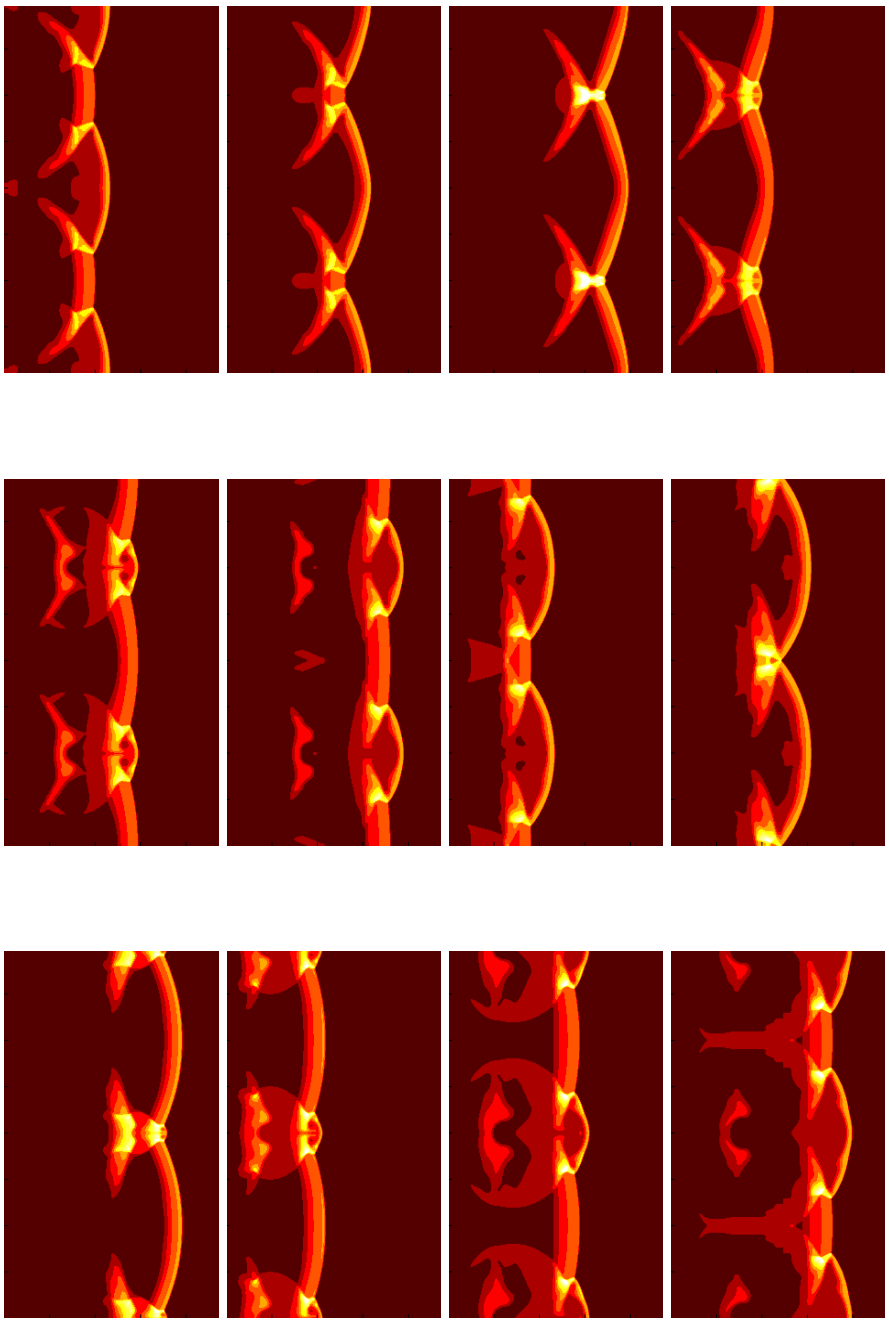

FIG. 5.7. *Density distribution of the propagating detonation front at time* $t = 5/64, 6/64, ..., 16/64$ *(from left* $\rightarrow$ *right, top* $\rightarrow$ *bottom). The phenomena of "explosion within explosion" can be clearly observed at the leading shock front.*